CrossMark

ORIGINAL ARTICLE

Structural reorganization of pyramidal neurons in the medial prefrontal cortex of alcohol dependent rats is associated with altered glial plasticity

Airee Kim · Eva R. Zamora-Martinez ·
Scott Edwards · Chitra D. Mandyam

Abstract In rodents, chronic intermittent ethanol vapor exposure (CIE) produces alcohol dependence, alters the activity of pyramidal neurons and decreases the number of glial progenitors in the medial prefrontal cortex (mPFC). Adult male Wistar rats were exposed to CIE and were injected with mitotic markers to label and phenotype proliferating cells to test the hypothesis that CIE produces concurrent alterations in the structure of pyramidal neurons and the cell cycle kinetics and developmental stages of glial progenitors in the mPFC. Medial prefrontal cortical tissue was processed for Golgi-Cox staining, immunohistochemistry and Western blotting analysis. CIE increased dendritic arborization and spine densities within basal and apical dendrites of pyramidal neurons via aberrant reorganization of actin cytoskeleton-associated molecules. CIE concomitantly increased the expression of total NR2B subunits without affecting phosphorylation of NR2B at Tyr-1472 or levels of PSD-95. CIE reduced the length of S-phase of the cell cycle of glial progenitors and reduced proliferation and differentiation of progenitors into bHLH transcription factor Olig2-expressing premyelinating oligodendrocyte progenitor cells (OPCs). CIE also produced a corresponding hyperphosphorylation of Olig2, and reduced expression of myelin basic protein. Our findings demonstrate that CIE-induced alterations in OPCs and myelin-related proteins are associated with profound alterations in the structure of pyramidal neurons. In sum, our results not only provide evidence that alcohol dependence leads to pathological changes in the mPFC, which may in part define a cellular basis for cognitive impairments associated with alcoholism, but also show dependence-associated morphological changes in the PFC at the single neuron level.

Keywords Chronic ethanol · Vapor-induced dependence · BrdU · IdU · CldU · Olig2 · MBP

A. Kim · E. R. Zamora-Martinez · C. D. Mandyam (✉)
Committee on the Neurobiology of Addictive Disorders, The
Scripps Research Institute, 10550 North Torrey Pines Road,
SP30-2400, La Jolla, CA 92037, USA
e-mail: cmandyam@scripps.edu

S. Edwards
Department of Physiology, Alcohol and Drug Abuse Center of
Excellence, LSU Health Sciences Center, New Orleans, LA,
USA

C. D. Mandyam
Skaggs School of Pharmaceutical Sciences, University of
California San Diego, La Jolla, CA, USA

Introduction

Alcoholism in humans impairs the structure of, and function dependent on, the frontal cortex (Bechara et al. 2001; George et al. 2001; Tapert et al. 2004a, b; De Bellis et al. 2005; Medina et al. 2008; Squeglia et al. 2012; Bava et al. 2013; Seo et al. 2013), but the underlying cellular mechanisms contributing to these deleterious effects are unclear. For example, alcoholics show deficits in executive function, declarative memory, and impulsivity, effects that indicate frontal cortex dysfunction (Parsons and Nixon 1993; Sullivan et al. 2000; Bechara et al. 2001). These deficits are associated with neurodegeneration and loss of myelin (Lewohl et al. 2005; Pfefferbaum and Sullivan 2005; Ridge et al. 2008; Jacobus et al. 2009; McQueeny et al. 2009; MacKay et al. 2011; Skuja et al. 2012; Bava et al. 2013), suggesting alterations in structure and function of the frontal cortex. Investigating the effects of chronic alcohol exposure on cortical neural systems and myelin in

rodent models can help elucidate the neurobiological changes contributing to the pathology of alcoholism in humans (Heilig and Egli 2006).

Early in vitro studies have reported that chronic intermittent ethanol exposure alters the kinetics and function of N-methyl-D-aspartate-type glutamate receptors (NMDARs) in cortical neurons and these effects were associated with enhanced expression of NMDA receptor subunit 2B [NR2B; (Hu and Ticku 1995; Hu et al. 1996)]. Recent ex vivo slice physiology studies in the medial prefrontal cortex (mPFC) have demonstrated that acute ethanol treatment decreases sustained depolarization that occurs in pyramidal neurons during up-states, indicating that ethanol decreases NMDAR-mediated excitatory postsynaptic currents (Tu et al. 2007; Weitlauf and Woodward 2008; Woodward and Pava 2009). Such mechanistic studies have been extended in animal models of chronic ethanol exposure to demonstrate that ethanol alters the functional and structural plasticity of pyramidal neurons in the mPFC. For example, chronic intermittent ethanol vapor exposure (CIE) produces significant, yet opposing effects on pyramidal neuron synaptic activity (persistent increase in NMDAR-mediated excitatory postsynaptic currents), and synaptic plasticity (aberrant increase in NMDAR-mediated spike timing-dependent plasticity) compared with acute effects on slices, possibly through an NR1- and NR2B-mediated mechanism (Kroener et al. 2012). These adaptive changes in NMDARs during long-term ethanol exposure may be occurring to counterbalance the initial prolonged inhibitory effects of ethanol on NMDAR activity, and may contribute to the aberrant neuronal excitability and neuronal toxicity observed during withdrawal and protracted abstinence (Grant et al. 1990; Chandler 2003; Kroener et al. 2012). Notably, the altered function of pyramidal neurons is associated with altered structure of pyramidal neurons (increased dendritic arborization and mature spine density), suggesting dysfunctional cortical networking in the mPFC (Holmes et al. 2012; Kroener et al. 2012). Furthermore, CIE alters certain behavioral measures dependent on the PFC, namely, attentional set-shifting and extinction encoding, suggesting maladaptive behavioral flexibility (Holmes et al. 2012; Kroener et al. 2012); these deficits may contribute to the cognitive impairments and loss of behavioral control seen in alcohol-dependent subjects.

Gliogenesis and neurogenesis in the adult brain have been conceptualized to be brain regenerative mechanisms; whether the newly born glia and neurons replace diseased cells or dying cells is a question receiving intense focus. In this context, particularly interesting is the capacity of the mPFC to generate newly born glia, endothelial cells and neurons (Mandyam and Koob 2012). The number of progenitors in the mPFC that develop into glial fibrillary acidic protein (GFAP) + astroglia is fewer compared with neuron-glia 2 (NG2) + glia [also known as oligodendrocyte progenitor cells (OPCs), polydendrocytes or synantocytes] (Mandyam and Koob 2012); however, the functional significance of NG2 gliogenesis in the adult mPFC is unknown. Emerging studies from several in vitro and in vivo models show that NG2 glia differentiate into pre-myelinating oligodendrocytes, mediate nonsynaptic events, and may assist with neuronal transmission (Butt et al. 2002; Watanabe et al. 2002; Belachew et al. 2003; Dawson et al. 2003; Ligon et al. 2006; Rivers et al. 2008; Allen and Barres 2009; Kang et al. 2010; Sun et al. 2011). These findings have led to proposals that stimulus-related changes in central nervous system myelin could be considered a form of neural plasticity, whereby (presumably active) axons and dendrites undergo myelination (through NG2 gliogenesis) to improve the speed and efficiency of nerve conduction, thus strengthening or synchronizing specific neuronal networks (Fields 2005, 2010). We have recently demonstrated that CIE reduces the number of newly born progenitors and their capacity to survive in the mPFC (Richardson et al. 2009), suggesting that ethanol's effect on function and structure of pyramidal neurons in the mPFC could be due to ethanol's neurotoxicity as revealed by inhibition of mPFC progenitors and gliogenesis. Together, these prior observations lead us to the hypothesis that CIE produces structural reorganization of mPFC pyramidal neurons by reducing the number of myelinating oligodendrocytes and expression of myelin in the mPFC. Golgi-Cox staining was used to determine the structure of pyramidal neurons, and Western blot analysis was used to determine changes in proteins associated with maintaining activity of neurons and myelinating glia. Rats were injected with 5-bromo (iodo or chloro)-2′-deoxyuridine (BrdU/IdU or CldU) to label proliferating synthesis (S)-phase progenitors and euthanized 2 h later to measure cell proliferation and cell cycle kinetics and 28 days later to measure cell survival.

Methods

Animals

Adult male Wistar rats (Charles River), weighing 225–275 g and 8 weeks old at the beginning of the experiments, were housed in groups of 2–3 per cage in a temperature-controlled (22 °C) vivarium on a 12 h/12 h light/dark cycle (lights on at 8:00 P.M.) with ad libitum access to food and water. All procedures were performed during the dark phase of the light/dark cycle. Thirty-nine rats completed the study (experimental design in Table 1). Experimental procedures were conducted in strict adherence to the

Table 1 Experimental design and number of animals in each study

Experimental design	Number of animals		
Study	Control	CIE	BALs indicated in figure
Western blotting + Golgi Cox	6	6	1a
Western blotting only		6	1a
IdU/CldU	4	6	1b
Brdu	4	7	1c
Total	14	25	

National Institutes of Health Guide for the Care and Use of Laboratory Animals (NIH publication number 85–23, revised 1996) and approved by the Institutional Animal Care and Use Committee of The Scripps Research Institute.

Dependence induction by alcohol vapor chambers

A recent modification of the alcohol dependence model was made to reflect the natural progression of alcohol dependence in which ethanol exposure occurs in a series of extended exposures followed by periods of withdrawal (O'Dell et al. 2004; Gilpin et al. 2008). Chronic exposure to intermittent ethanol vapor exposure elicits even higher alcohol self-administration than continuous vapor (O'Dell et al. 2004), therefore, the intermittent procedure was used to induce dependence in alcohol-naïve animals in the present study. Vapors were delivered on a 14 h on/10 h off schedule for 7–10 weeks (Fig. 1). This schedule of exposure has been shown to induce physical dependence (Richardson et al. 2008). In the chambers, 95 % alcohol flows from a large reservoir to a peristaltic pump (model QG-6, FMI Laboratory, Fluid Metering). Alcohol is delivered from the pump to a sidearm flask at a flow rate that can be regulated. The flask is placed on a heater in which the drops of alcohol hitting the bottom of the flask

are vaporized. Air flow controlled by a pressure gauge is delivered to the flask and carries the alcohol vapors to the vapor chamber that contains the animal cages. The flow rate was set to deliver vapors that result in blood alcohol levels between 125 and 250 mg% (Fig. 1) or 27.2 and 54.4 mM (Gilpin et al. 2008). In this model, rats exhibit somatic withdrawal signs and negative emotional symptoms reflected by anxiety-like responses, hyperalgesia, and elevated brain reward thresholds (Schulteis et al. 1995; Roberts et al. 2000; Valdez et al. 2002; Rimondini et al. 2003; O'Dell et al. 2004; Zhao et al. 2007; Sommer et al. 2008; Edwards et al. 2012; Vendruscolo et al. 2012). Control rats were not exposed to alcohol vapor.

Measurement of blood alcohol levels

Blood sampling (tail bleedings) was performed immediately after daily bouts of alcohol vapor exposure in dependent animals twice during the first week of vapor exposure and once during each subsequent week of vapor exposure. Plasma (5 µl) was used for measurement of blood alcohol levels using an Analox AM 1 analyzer (Analox Instruments). The reaction is based on the oxidation of alcohol by alcohol oxidase in the presence of molecular oxygen (alcohol + O_2 → acetaldehyde + H_2O_2). The rate of oxygen consumption is directly proportional to the alcohol concentration. Single-point calibrations were done for each set of samples with reagents provided by Analox Instruments (25–400 mg% or 5.4–87.0 mM). When blood samples were outside the target range (125–250 mg%), vapor levels were adjusted.

Golgi-Cox staining and analysis to determine the structure of mPFC pyramidal neurons

For determination of the effect of alcohol dependence on cortical pyramidal neuronal architecture, a group of vapor-exposed rats ($n = 6$) and controls ($n = 6$) were killed by rapid decapitation under light isoflurane anesthesia 3 h after the last vapor exposure and whole brain was quickly
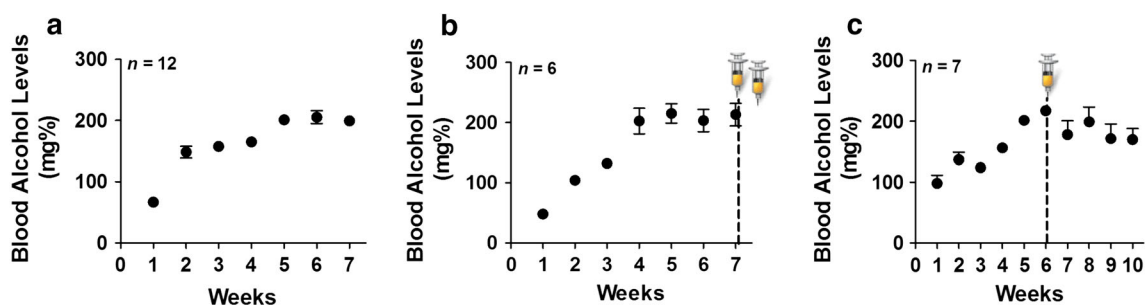

Fig. 1 Steady blood alcohol levels (BALs) can be maintained via chronic intermittent ethanol vapor exposure paradigm. **a–c** BALs expressed in mg% over several weeks of CIE. **a** BALs from animals used for Golgi-Cox and Western blotting analysis; **b** BALs from animals used for CldU/IdU cell cycle kinetics analysis; **c** BALs from animals used for BrdU/Olig2 analysis. Syringes in **b**, **c** indicate the time point when IdU/CldU (**b**) or BrdU (**c**) were injected
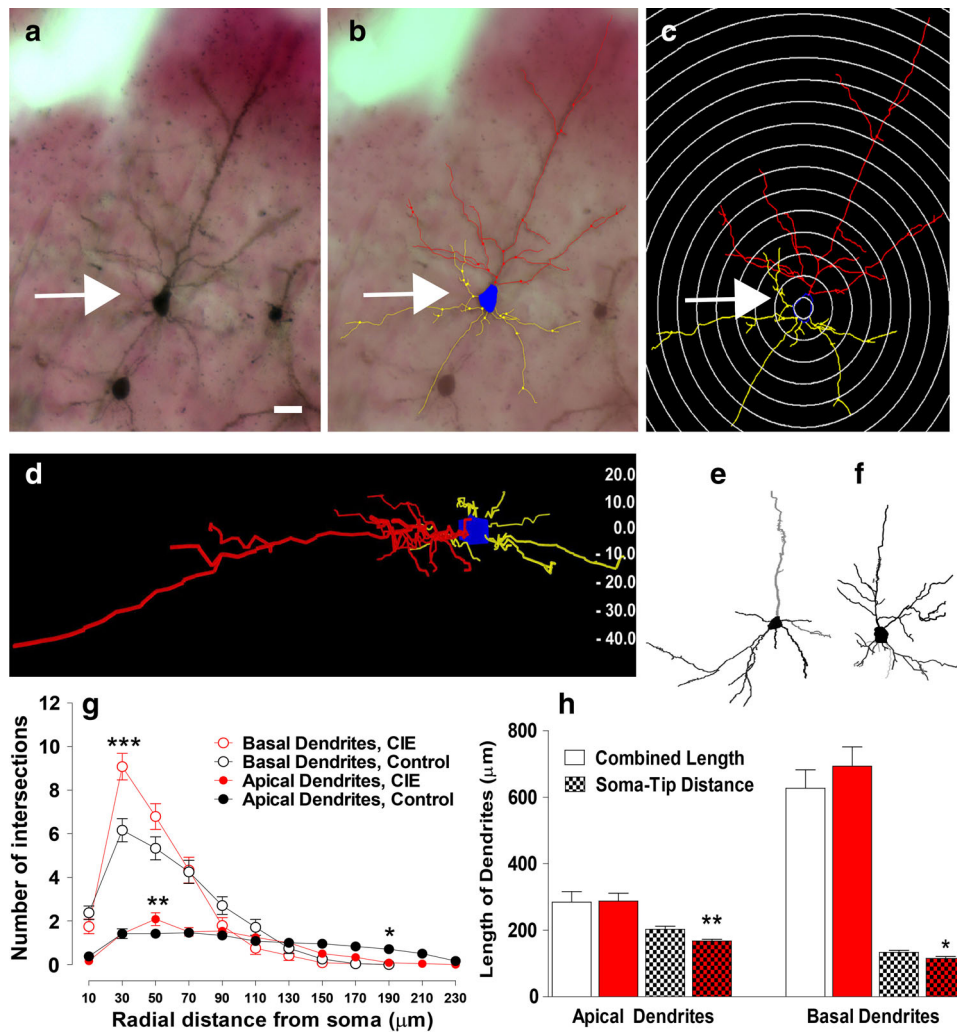
Fig. 2 CIE alters the structure of pyramidal neurons in the mPFC. a–d 3D reconstruction and Sholl ring analysis at 20 μm ring distance with a starting ring at 10 μm. A representative example of Golgi-Cox stained pyramidal neuron in the mPFC (a) along with neuron tracings in Neurolucida (b) and corresponding 3D reconstruction and Sholl ring (c) from one CIE animal. *xyz* orientation of the cell in (a) and the corresponding depth of the cell shown in micrometers are indicated in (d). *xyz* analysis indicated that the entire cell in its *xyz* axis is within 60 μm thickness. e, f Neuron tracings from one control (e) and one CIE (f) animal. g Total number of intersections of basal dendrites (*filled circles*, control in *black* and CIE in *red*) and apical dendrites (*open circles*, control in *black* and CIE in *red*) of mPFC pyramidal neurons. h Length of basal and apical dendrites shown as soma to tip distance of the dendrites or total length of all dendritic branches; controls are in *black* and CIE is in *red*. $n = 6$ animals in each group and neuron data is from 24 neurons in each group. $***p < 0.001$, $**p < 0.01$, $*p < 0.05$ compared with controls

removed and cut mid-sagitally. One half of the brain (the left hemisphere for each animal in control and CIE groups) was processed for Golgi-Cox staining. The other half (right hemisphere) was used for Western blotting analysis. For Golgi-Cox staining, the brain was submerged in Golgi-Cox solution A + B (FD Neurotechnologies Inc.) for 8 days at room temperature, followed by solution C for 4 days at room temperature and stored at −80 °C until processed for staining. Frozen brain tissue was coronally cut on a cryostat at 100-μm-thick sections and stained with solution D + E and dehydrated according to manufacturer's instructions. Brains were coded before sectioning to ensure that experimenters were blind to treatments.

To evaluate pyramidal neuron morphology, a Zeiss Axiophot microscope and a computer-based system (Neurolucida; Micro-BrightField) were used to generate three-dimensional neuron tracings that were subsequently visualized and analyzed using NeuroExplorer (MicroBright-Field). For a neuron to be selected, the following four criteria were met: (1) the pyramidal neuron was in the layer 2/3 of the medial prefrontal cortex, (2) the pyramidal neuron was distinct from other pyramidal and interneurons to allow for identification of dendrites, (3) the pyramidal neuron was not truncated, and (4) the pyramidal neuron exhibited dark, well-filled staining throughout (Gould et al. 1990).
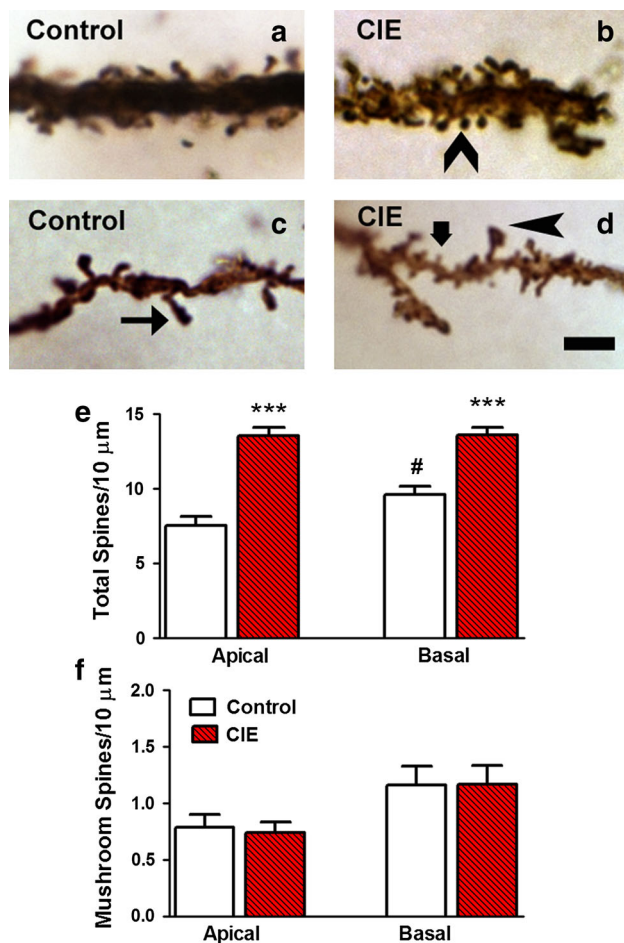
Fig. 3 CIE increases the spine density of pyramidal neurons in the mPFC. **a–d** Representative images of 10 μm segments of apical (**a**, **b**) and basal (**c**, **d**) dendrites from distal portions of the dendrite from one control (**a**, **c**) and one CIE (**b**, **d**) animal. *Arrowhead* in (**b**), *thin arrow* in (**c**) and *thick arrow* in (**d**) point to nonmushroom-type spines. *Arrowhead* in (**d**) points to mushroom-type spine. *Scale bar* in (**d**) is 2 μm, applies (**a–d**). **e**, **f** Quantitative analysis of total number of spines (nonmushroom + mushroom type; **e**) and mushroom-type spines (**f**) from control (*open bars*) and CIE (*red hatched bars*) animals from apical and basal dendrites. $n = 6$ animals in each group and spine data is from 24 neurons in each group. ***$p < 0.001$ compared with controls, #$p < 0.05$ compared with apical dendrites

For each animal, four pyramidal neurons in layer 2/3 of the medial prefrontal cortex (3.7–2.0 mm from bregma; infralimbic and prelimbic cortices were combined) were traced at 40× magnification with an oil immersion lens (equipped with a 10× eye piece). Both the apical and basal trees were traced, and morphological measurements were analyzed separately. For each reconstructed neuron, an estimate of dendritic complexity was obtained using the Sholl ring method. A 3D Sholl analysis was performed in which concentric spheres of increasing radius (starting sphere 10 μm and increasing in 20 μm increments) were layered around the cell body until dendrites were completely encompassed (Fig. 2c). The number of dendritic

intersections at each increment was counted, and results were expressed as total intersections and the number of intersections per radial distance from the soma.

For all neurons, spine density was measured at 63–100× magnification with an oil immersion lens (equipped with a 10× eye piece) on the same dendritic branches used for Sholl analysis. Dendritic spine density was measured on four dendritic segments from both the basal and apical tree. For the basal tree, spines were counted along 10–12 μm segments of 2°–5° order branches located at least 50 μm away from the cell body. For the apical tree, spines were counted along 10 μm segments of primary apical branches located at least 80 μm away from the cell body. Dendritic spines were classified into two categories (mushroom or nonmushroom) based on their length and neck and head width (Fig. 3a–d). Stringent criteria were used for the categorization of spine heads into mushroom- and nonmushroom-type spines and were based on several seminal reports (Peters and Kaiserman-Abramof 1970; Harris et al. 1992; Markham et al. 2005; Jurgens et al. 2012). All measurements of spine density were taken from 1- to 2-μm-thick dendritic segments to minimize the number of spines hidden by the dendritic shaft and ensure that the number of hidden spines was proportional across all segments counted and among treatment groups. The total number of dendritic spines visible along both sides of the segment was counted and expressed as number of spines per 10 μm of dendrite.

Western blotting

Procedures optimized for measuring neuronal levels of both phosphoproteins and total proteins were employed (Edwards et al. 2013). Tissue punches from alcohol naive rats ($n = 6$) and alcohol dependent rats ($n = 12$) from 500-μm-thick PFC sections were homogenized on ice by sonication in buffer (320 mM sucrose, 5 mM HEPES, 1 mM EGTA, 1 mM EDTA, 1 % SDS, with Protease Inhibitor Cocktail and Phosphatase Inhibitor Cocktails II and III diluted 1:100; Sigma), heated at 100 °C for 5 min, and stored at −80 °C until determination of protein concentration by a detergent-compatible Lowry method (Bio-Rad, Hercules, CA). Samples were mixed (1:1) with a Laemmli sample buffer containing β-mercaptoethanol. Each sample containing protein from one animal was run (10–30 μg per lane) on 8–12 % SDS-PAGE gels (Bio-Rad) and transferred to polyvinylidene fluoride membranes (PVDF pore size 0.2 μm). Blots were blocked with 5 % milk (w/v) in TBST (25 mM Tris–HCl (pH 7.4), 150 mM NaCl and 0.1 % Tween 20 (v/v)) for 16–20 h at 4 °C and were incubated with the primary antibody for 16–20 h at 4 °C: antibody to NR2B (1:200, Santa Cruz cat. no. sc-9057, predicted molecular weight 178 kDa, observed band ∼180 kDa), antibody to pNR2B Tyr-1472 (1:200, Cell

Signaling cat. no. 4208S, predicted molecular weight 190 kDa, observed band ∼180 kDa), antibody to Arp2/3 (1:500, Millipore, cat. no. MABT95, predicted molecular weight 20 kDa, observed band ∼23 kDa), antibody to neuronal Wiskott–Aldrich Syndrome protein (nWASP; 1:500, Cell Signaling, cat. no. 4848S, predicted molecular weight ∼60 kDa, observed band ∼60 kDa), antibody to PSD-95 (1:500, Millipore, cat. no. 04-1066, predicted band size 95 kDa, observed band ∼95 kDa), antibody to oligodendrocyte lineage transcription factor 2 [Olig2; 1:10,000, predicted molecular weight 37 kDa (Ligon et al. 2006), observed band ∼37 kDa], antibody to phosphorylated Olig2 (pOlig2) Ser-10, 13,14 [1:500, predicted molecular weight 35 kDa, observed band ∼35 kDa (Sun et al. 2011)], antibody to MBP (1:500, Abcam, cat. no. ab40390, predicted band size 18–23 kDa, observed band ∼20 kDa). β-tubulin (1:8,000, Santa cruz cat. no. sc-5274, predicted band size 50 kDa, observed band ∼50 kDa) was used as a loading control. Blots were then washed three times for 15 min in TBST, and then incubated for 1 h at room temperature (24 °C), appropriately with either horseradish peroxide-conjugated goat antibody to rabbit (1:10,000, BioRad) or horseradish peroxide-conjugated goat antibody to mouse IgG1 (1:10,000, BioRad) in TBST. After another three washes for 15 min with TBST, immunoreactivity was detected using SuperSignal West Dura chemiluminescence detection reagent (Thermo Scientific) and collected using HyBlot CL Autoradiography film (Denville Scientific) and a Kodak film processor. Net intensity values were determined using the ImageJ software (version 1.45S, NIH). Following chemiluminescence detection, blots were stripped for 20 min at room temperature (Restore, Thermo Scientific) and reprobed for total protein levels of β-tubulin for normalization purposes. Unpaired Student's *t* tests were used to compare values between groups.

Injections of mitotic markers

Cell cycle kinetics group

Alcohol naïve (control, $n = 4$) and alcohol dependent rats ($n = 6$) 2 h after the last vapor exposure received one injection of 50 mg/kg 5-Iodo-2′-deoxyuridine (IdU; MP Biomedicals, cat# 100357; dissolved in 0.9 % saline, 0.2 N NaOH at 2.5 mg/ml, normalized to pH 7 with 10 N HCl) followed by 50 mg/kg CldU 2 h later (Yuan et al. 2011). These rats survived for 30 min after the CldU injection and were killed by transcardial perfusions.

Cell survival group

A separate group of alcohol naive rats ($n = 4$) and alcohol dependent rats ($n = 7$) received one injection of 150 mg/kg BrdU 2 h after the vapor exposure. The alcohol dependent rats continued to receive ethanol vapors for additional 4 weeks and were killed by transcardial perfusions 3–4 h after the last vapor exposure.

Perfusions and brain tissue collection

After the last vapor exposure, rats were fully anesthetized using chloral hydrate (240 mg/kg, i.p.). Rats were then transcardially perfused with phosphate-buffered saline (over 2 min at 15 ml/min) and 4 % paraformaldehyde (over 20 min at 15 ml/min). The brains were dissected out and postfixed in 4 % paraformaldehyde at 4 °C for 16–20 h and sectioned in the coronal plane at a thickness of 40 μm on a freezing microtome. The sections through the brain were collected in nine vials [containing 0.1 % NaN₃ in 1× phosphate-buffered saline (PBS)] and stored at 4 °C. One-ninth of the brain region was used for immunohistochemical analysis.

Antibodies, immunohistochemistry, microscopic analysis, and quantification

The following primary antibodies were used for immunohistochemistry (IHC): mouse monoclonal anti-BrdU (1:10, catalog # ab8152, Abcam), rat monoclonal anti-BrdU (1:400; catalog # MCA2060, Serotec) and rabbit polyclonal anti-Olig2 (1:10,000). The left and right hemispheres of every ninth section through the rat medial prefrontal cortex (Fig. 5a) were slide-mounted, coded, and dried overnight prior to IHC. The sections were pretreated (Mandyam et al. 2004), blocked, and incubated with the primary antibodies followed by biotin-tagged (Olig2) or fluorescent-tagged (CldU, IdU, BrdU and Olig2) secondary antibodies. Absolute cell counting [as demonstrated in Noori and Fornal, (Noori and Fornal 2011)] rather than unbiased stereological estimates in sections through the mPFC [Fig. 5a; mPFC; 3.7–2.2 mm from bregma; (Paxinos and Watson 1997)] was quantified with a Zeiss Axiophot Microscope equipped with MicroBrightField Stereo Investigator software, a three-axis Mac 5000 motorized stage, a Zeiss digital charge-coupled device ZVS video camera, PCI color frame grabber, and computer workstation. Live video images were used to draw contours delineating the mPFC and were traced with 2.5× objective (equipped with 10× eyepiece). Cell counting was performed visually by the observer blind to the study with a 40× objective (equipped with a 10× eyepiece). A 150 × 150 μm frame was placed over the regions of interest using the Stereo Investigator stereology platform. The frame was moved systematically over the tissue to cover the entire contoured area and labeled cells in each region falling entirely within the borders of the contour

were marked and analyzed. Immunoreactive cells were quantified bilaterally from sections representing 3.7, 3.2, 2.7, and 2.2 mm from bregma and were summed up for each brain region. Cells in the mPFC were summed and multiplied by nine to give the total number of cells (Mandyam et al. 2007).

Length of S-phase

Fluorescent double labeling of CldU/IdU was performed for S-phase analysis as described previously (Yuan et al. 2011). To determine the S-phase of the cell cycle, proliferating cells in the S-phase were pulse-chased with low doses of exogenous markers IdU and CldU (50 mg/kg each, i.p.); (Maslov et al. 2004; Burns and Kuan 2005; Vega and Peterson 2005; Breunig et al. 2007), and the length of the S-phase was calculated using the parameters according to Cameron and McKay (Cameron and McKay 2001) and Hayes and Nowakowski (Hayes and Nowakowski 2002). IdU and CIdU (Fig. 5b–h) were used sequentially to label S-phase cells at two time points ($T_1 = 0$ h, $T_2 = 2$ h), a time point predicted to be less than the G_2/M-phase based on cell cycle studies in the rat hippocampus; (Cameron and McKay 2001). Control and CIE rats were given one injection of IdU followed by CIdU 2 h (T_2) later after 7 weeks of chronic CIE. Every ninth section through the mPFC was used for analysis. We used a mouse monoclonal anti-BrdU antibody from Abcam (1:10; cat# ab8152) to detect IdU cells and a rat monoclonal anti-BrdU antibody from Serotec (1:400; cat# MCA2060) to detect CldU cells (Yuan et al. 2011). The lack of nonspecific staining was confirmed in a separate set of animals that received either IdU injections only or CldU injections only (data not shown). In addition, both the antibodies for IdU and CldU showed specific staining in brain tissue from BrdU-injected rats (data not shown).

Fluorescently labeled brain tissue from animals sequentially injected with IdU and CldU (CY3 for IdU and CY2 for CldU, respectively; Fig. 5b–h) revealed three distinct populations of proliferating cells in the S-phase, some cells labeled with rat antibody only, some labeled with mouse antibody only, and most colabeled with both antibodies (Fig. 5b–e). The labeling pattern was quantified as the following: single-labeled IdU (number of cells that exit the S-phase during $T_2 = 2$ h, N_{EX}), single-labeled CldU (number of cells that enter the S-phase during $T_{CldU} = 30$ min, N_{EN}), and double-labeled IdU/CldU cells. Based on previous reports, the expected value (E) of the proportion of dividing cells in the S-phase at any given time point was equal to the proportion of cell cycle time of the S-phase labeled with a single S-phase marker (Nowakowski et al. 1989; Hayes and Nowakowski 2000; Cameron and McKay 2001; Yuan et al. 2011).

Therefore, $E\left\{\dfrac{N_{EX}}{N_S}\right\} = \dfrac{T_{EX}}{T_S}$

The calculation of the length of the S-phase (T_S) was performed as the following:

$T_{EX} = T_2$ = interinterval time (2 h; Fig. 5f).

Total number of cells labeled with mouse BrdU antibody (IdU) = $N_{IdU.}$

Total number of cells labeled with rat BrdU antibody = CldU cells = cells in S-phase.

$N_S = N_{CldU}$

Cells that exited the S-phase and entered the G_2/M-phase at $T_2 = (N_{IdU\ single}) = N_{EX.}$

Time-line of S-phase $T_S = T_2/(N_{EX}/N_C)$.

T_S values were calculated individually for each rat.

Number of S-phase cells

The number of CldU-immunoreactive (IR) cells was quantified from each control and CIE rat in every ninth section through the mPFC using a stereology platform. The number of cells was multiplied by nine to give an estimate for the total number of cells in the S-phase of the cell cycle per mm² of the mPFC.

Cell survival study

Every ninth section through the mPFC from control and CIE rats that received BrdU was mounted and stained for BrdU (CY3) and Olig2 (FITC). All BrdU-labeled cells (15–22 cells) from each rat were processed for confocal microscopy to determine the ratio of BrdU/Olig2 colabeling.

Confocal microscopy

Confocal analysis was performed on individual CldU-immunoreactive (IR), IdU-IR and BrdU-IR cells using a $60\times$ oil immersion objective (equipped with a $10\times$ eyepiece). Optical sectioning in the z-plane was performed using multitrack scanning with a section thickness of 0.45 μm. Colocalization of antibodies was assessed with the confocal system by analysis of adjacent z-sections (gallery function and orthogonal function for equal penetration of the antibodies). For the S-phase study, the number of cells that were IdU alone, CldU alone, and IdU/CldU-labeled were quantified and are shown as raw data for each animal. For cell survival study, the number of BrdU cells colabeled with Olig2 was estimated and the percent of BrdU cells colabeled with Olig2 in each rat was used for analysis.

Statistical analysis

The effects of group (control vs. CIE) and distance from the soma on dendritic length were analyzed using two-factor ANOVA, with repeated measures for distance from the soma, followed by Fisher's LSD post hoc tests. Unpaired Student's t tests were used to compare overall apical length between groups. Differences in cell cycle kinetics, number of progenitors and density of proteins were also analyzed by Student's t tests. Data are expressed as mean $\pm$ SEM. Values of $p < 0.05$ were considered statistically significant. Graphs were generated using GraphPad Prism 5.0 software. Images presented here were collected on a confocal microscope (LaserSharp 2000, version 5.2, emission wavelengths 488, 568, and 647 nm; Bio-Rad Laboratories) and imported into Photoshop (version CS2). Only the gamma adjustment in the Levels function was used.

Results

Chronic inhalation of ethanol vapors over an intermittent schedule produces and maintains robust blood alcohol levels

Measurements of experimenter-adjusted blood alcohol levels (BALs) indicated an increase over the 6–7 weeks compared with the first week of vapor exposure in the groups of animals assigned for Western blotting analysis, the IdU/CldU study and the BrdU study [$F(6, 114) = 63.9$, $p < 0.001$ (Fig. 1a–c)] by repeated measures two-way ANOVA). Although the flow rate was set to deliver ethanol vapors that result in BALs between 125 and 250 mg%, this level was not reached in the first week of vapor exposure in certain animals. However, BALs were not significantly different between the groups [$F(2, 114) = 0.16$, n.s. (Fig. 1a–c)] and was maintained between 150 and 250 mg% (target BAL) during weeks 4–7 until week 10.

CIE produces significant alterations in the structure of pyramidal neurons in the mPFC

Dendritic arborization

Both the apical and basal trees of mPFC pyramidal neurons were traced, and morphological measurements were analyzed separately (Fig. 2a–f). Morphological analysis demonstrated that the total number of dendritic intersections in the basal dendrites were significantly higher when compared with apical dendrites. A two-way ANOVA revealed a main effect of type of dendrite [Fig. 2g; $F(1, 736) = 95.5$, $p < 0.001$], and a significant interaction [type of dendrite $\times$ distance from soma; $F(15, 736) = 30.4$, $p = 0.001$], indicating that the number of intersections varied over the distance from soma. CIE increased the number of dendritic intersections in the basal dendrites. A two-way ANOVA revealed a significant effect of ethanol [Fig. 2g; $F(1, 460) = 4.2$, $p = 0.04$], and a significant interaction (ethanol $\times$ distance from soma; $F(9, 460) = 5.9$, $p < 0.001$]. CIE also increased the number of dendritic intersections in the apical dendrites. A two-way ANOVA revealed a significant effect of ethanol [Fig. 2g; $F(1, 736) = 4.3$, $p = 0.03$], and a significant interaction [ethanol $\times$ distance from soma; $F(15, 736) = 3.3$, $p < 0.001$]. Post hoc analyses indicated higher number of intersections at distances 20–60 μm from the soma in both basal and apical dendrites in CIE animals compared with controls (Fig. 2g, $p < 0.01$), indicating an increase in dendritic extent near the soma.

Dendritic length

CIE did not alter the total combined length of the apical and basal dendritic trees, but significantly reduced the soma-tip distance of the apical and basal dendritic trees (Fig. 2h; $p < 0.05$), indicating dendritic retraction.

Dendritic spine density

Spine density was calculated and analyzed separately for apical and basal dendritic trees. A two-way ANOVA revealed a main effect of the number of spines on type of dendrite [Fig. 3e; $F(1, 92) = 3.7$, $p = 0.05$], indicating more number of spines on the basal dendrites compared with apical dendrites. CIE increased the spine density of mPFC apical and basal dendrites (Fig. 3a–d). A two-way ANOVA revealed a significant effect of ethanol [Fig. 3e; $F(1, 92) = 83.45$, $p = 0.0001$], and a strong trend for a significant interaction [ethanol $\times$ type of dendrite; $F(1, 92) = 3.5$, $p = 0.06$]. There were no differences in the number of mushroom-like spines in apical dendrites when compared with basal dendrites and CIE did not alter the number of mushroom-like spines (Fig. 3f).

CIE alters the levels of NR2B NMDA receptor subunits in the mPFC

To determine the effects of CIE on the total levels and the phosphorylation state of NR2B subunits, Western blot analyses were carried out on mPFC-enriched tissue punches. Consistent with a previous report (Kroener et al. 2012), CIE significantly increased the levels of total NR2B subunits (Fig. 4a–b; $p = 0.04$ by Student's t test). Increases in total NR2B levels were not associated with enhanced phosphorylation of NR2B at Tyr-1472 (Fig. 4a–b).

Fig. 4 CIE increases levels of total NR2B without effecting phosphorylation of NR2B (pNR2B) at Tyr-1472 in the mPFC. **a** Representative immunoblots of total NR2B vs. pNR2B compared with β-tubulin. **b** Densitometric analysis of proteins in CIE animals expressed as percent change compared with controls. CIE elevates levels of Arp2/3 without effecting levels of PSD-95 and nWASP in the mPFC. **c** Representative immunoblots of Arp2/3 compared with β-tubulin. **d** Densitometric analysis of proteins in CIE animals expressed as percent change compared with controls. $n = 11$–12 in CIE group and six in controls; $*p \leq 0.05$ compared with controls
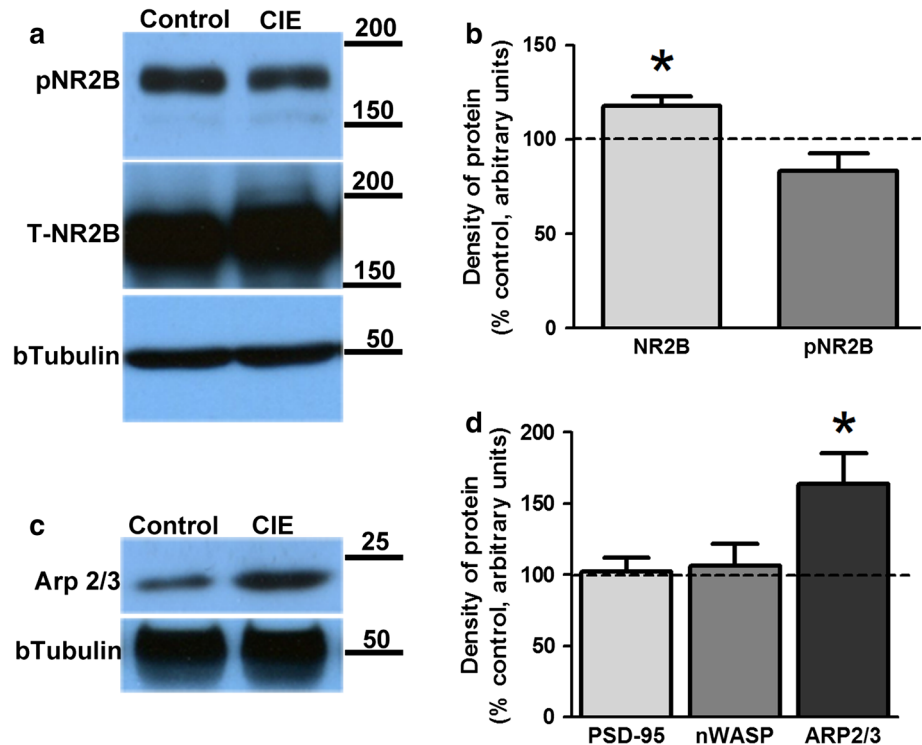
CIE alters the levels of actin nucleator complex Arp2/3 in the mPFC

To determine the effects of CIE on protein complexes that regulate actin cytoskeleton and microtubule formation that is necessary for the formation of filament protrusions or spines on dendrites, Western blot analyses were carried out to determine changes in the levels of PSD-95, Arp2/3 and nWASP, an activator of Arp2/3. Consistent with a recent report (Holmes et al. 2012), CIE did not alter levels of PSD-95 (Fig. 4d). CIE significantly increased levels of Arp2/3 (Fig. 4c, d; $p = 0.04$ by Student's t test) when compared with controls, although these changes were not associated with altered levels of nWASP (Fig. 4d).

CIE reduces the number of newly born glial progenitors in the mPFC by altering their cell cycle kinetics

Previous work from our laboratory demonstrated that IdU and CldU (analogs of BrdU) produce equivalent labeling of hippocampal progenitors compared with BrdU at lower doses (Yuan et al. 2011). We also demonstrated that in the hippocampus, IdU cells can be labeled with mouse monoclonal BrdU antibody, and CldU cells can be distinctly labeled with rat monoclonal BrdU antibody. In the mPFC, we demonstrate that sequential labeling with IdU followed by CldU displays three distinct populations of proliferating cells (Fig. 5b–e; g–i). We used this approach to determine the length of the S-phase of the cell cycle of

mPFC progenitors from the control and CIE groups. Animals were sequentially injected with IdU followed by CldU 2 h later (see Methods). According to our recently published mathematical calculations (Yuan et al. 2011), that is based on several seminal reports (Cameron and McKay 2001; Hayes and Nowakowski 2002), IdU+ cells in the S-phase at $T = 0$ h would have moved into the G_2/M phases of the cell cycle at $T = 2$ h when CldU was injected (Fig. 5f). At $T = 30$ min after CldU injection, CldU cells will mostly be in the S-phase (Fig. 5f). According to previously published reports, pulse-chasing S-phase cells at any given time point with two S-phase markers, such as [³H]thymidine and BrdU (Cameron and McKay 2001; Hayes and Nowakowski 2002) or IdU and CldU (Vega and Peterson 2005), produces three distinct populations of cells. For example, the set of S-phase cells labeled at $T_1 = 0$ h with IdU will be single (N_{EX}) and double labeled (N_S) at $T_2 = 2$ h (Fig. 5f). The set of S-phase cells labeled at $T_2 = 2$ h with CldU will be single (N_{EN}) and double labeled (N_S) when euthanized ($T_{CldU} = 30$ min; Fig. 5f). All three groups of S-phase cells were visible in all of the rats analyzed, with most of the S-phase cells double labeled with CldU and IdU (Fig. 5j–k). The calculation of the S-phase length in naive controls revealed a timeframe of >30 h (Fig. 5k), demonstrating that the S-phase of the cell cycle of mPFC progenitors is longer than the S-phase of hippocampal subgranular zone progenitors in adult rats (Olariu et al. 2007; Yuan et al. 2011). CIE did not alter the number of cells in N_{EN} and N_S, but showed a trend towards
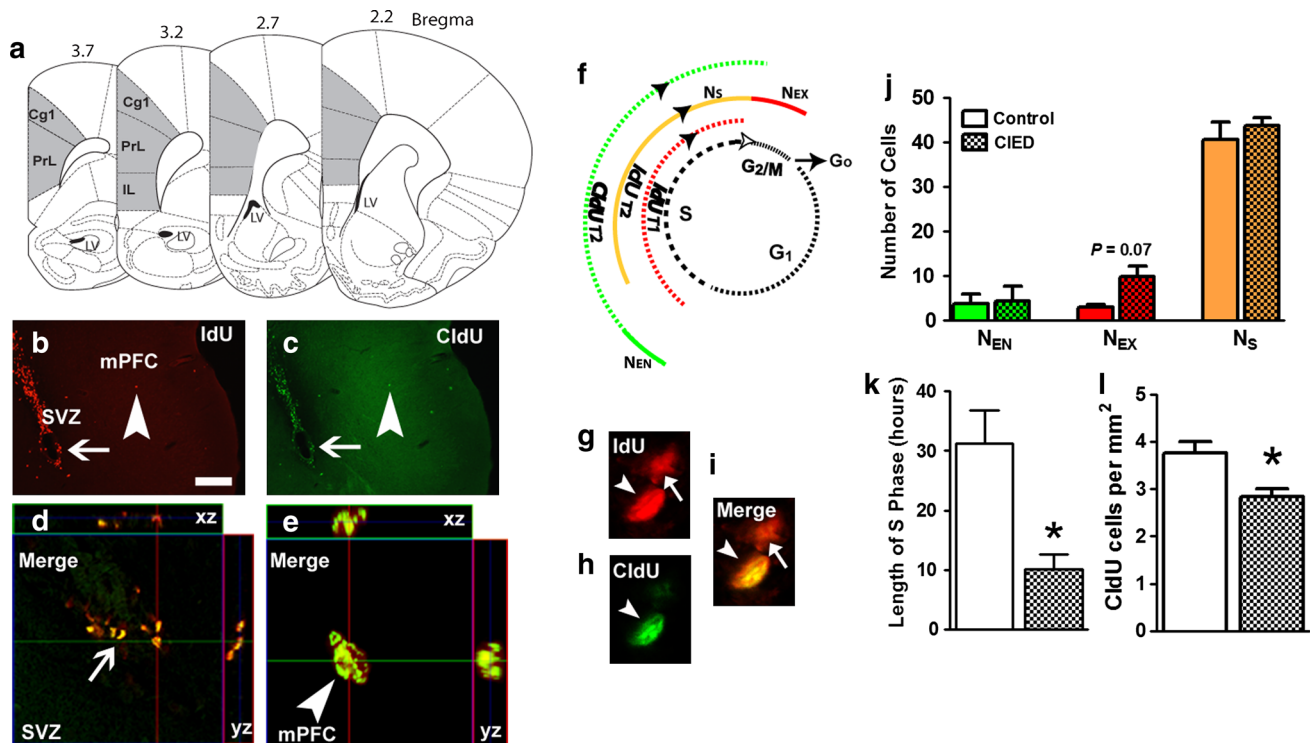
Fig. 5 CIE reduces the length of the S-phase of the cell cycle of mPFC progenitors. a Schematic of bregma regions and the area of prefrontal cortex included for quantification. Area shaded in *gray* included the cingulate cortex (Cg), prelimbic cortex (PrL), and infralimbic cortex (IL). Representative epifluorescent images of IdU (b) and CldU (c) labeling in the subventricular zone (SVZ) and mPFC from one control animal. *Thin arrow* in (b, c) points to cells in the SVZ and *arrowhead* in (b, c) points to a IdU/CldU double-labeled cell in the mPFC. Orthogonal view of IdU/CldU-labeled cells in the SVZ (d) and mPFC (e) showing equal penetration of antibodies in the *xz* and *yz* planes. f Schematic representation of the cell cycle of proliferating progenitors in the mPFC. S, synthesis phase; G_1, gap1

phase; G_2, gap2 phase and M, mitosis. N_S is number of cells in S-phase, N_{EX} is number of cells exiting the S-phase, N_{EN} is number of cells entering the S-phase of the cell cycle. Injections of IdU were given at T, time = 0 h and Cldu were given at $T = 2$ h. **g–i** Representative confocal images of IdU (*red*, g) and CldU (*green*, h) labeled cells in the mPFC from one control animal. j Quantitative analysis of number of IdU or CldU or IdU/CldU cells in the mPFC per animal from four pairs of bilateral mPFC sections. k Length of S-phase of proliferating progenitors in the mPFC expressed in hours. l Total number of CldU only cells in the mPFC represented as number of cells per mm^2 of the mPFC. $n = 6$ animals in each group. $*p < 0.05$ compared with controls

higher number of cells in N_{EX} ($p = 0.07$; Fig. 5j). S-phase analysis indicated that CIE decreased the duration of S-phase compared with controls (Fig. 5k; $p = 0.04$ by Student's *t* test). Separate stereological analysis of CldU + cells showed a significant reduction in the number of S-phase cells in CIE animals compared with controls (Fig. 5l; $p = 0.04$ by Student's *t* test).

CIE reduces the number of newly born and pre-existing premyelinating oligodendrocytes and levels of myelin basic protein in the mPFC by inducing hyperphosphorylation of the bHLH transcription factor Olig2

In controls and CIE animals, 28-day-old BrdU cells were colabeled with Olig2 (Fig. 6a–d). As expected, in the controls, ~60 % of BrdU cells were colabeled with Olig2, indicating that most of the progenitors in the mPFC differentiated into premyelinating oligodendrocytes (Fig. 6e).

CIE reduced the proportion of BrdU-labeled Olig2 cells (Fig. 6e; $p = 0.03$ by Student's *t* test). Immunohistochemistry of myelin basic protein showed no significant change in the location and morphology of myelin (Fig. 6f–g). Western blot analyses were performed to determine whether CIE reduced the total levels of Olig2 and whether CIE altered the phosphorylation of Olig2 (Fig. 6h). CIE reduced total Olig2 levels in the mPFC (Fig. 6i; $p = 0.02$ by Student's *t* test) and this reduction was associated with enhanced phosphorylation of Olig2 at Ser-10, 13, 14 (Fig. 6i; $p = 0.01$ by Student's *t* test). The reduction in premyelinating oligodendrocytes was also associated with lower levels of myelin basic protein (Fig. 6i; $p = 0.03$ by Student's *t* test).

Discussion

Exposure to chronic alcohol via the CIE paradigm provides several advantages for studying the neurobiological
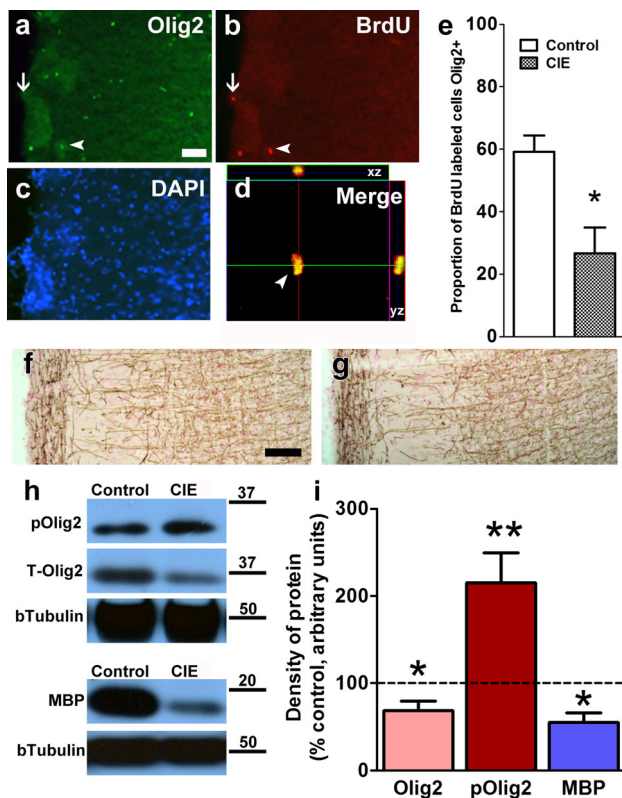
Fig. 6 CIE reduces the proportion of newly born Olig2 labeled cells in the mPFC and reduces myelin expression in the mPFC. **a–c** Epifluorescent images of mPFC cortex section stained for Olig2 (FITC, *green*, **a**), BrdU (CY3, *red*, **b**) and DAPI (*blue*, **c**). *Thin arrow* in (**a**, **b**) shows a BrdU-labeled cell that is not Olig2+. *Arrowhead* in (**a**, **b**) shows two BrdU-labeled cells that are Olig2+. **d** Orthogonal section of a BrdU+/Olig2+ cell in the mPFC [cell shown in (**b**)] showing equal penetration of the antibodies in *xz* and *yz* planes. **e** Ratio of 28-day-old BrdU+ cells colabeled with Olig2. **f**, **g** immunohistochemistry of myelin basic protein in the mPFC from one control (**f**) and one CIE (**g**) animal. **h** Representative immunoblots of phosphorylated Olig2 (pOlig2), total Olig2, MBP and corresponding blots for β-tubulin. **i** Densitometric analysis of total Olig2, pOlig2 and MBP in the mPFC represented as percent change from controls. $n = 7$ animals in CIE group and $n = 5$ animals in control group for Olig2/BrdU IHC analysis, and $n = 12$ animals in CIE group, $n = 6$ animals in control group for Western blotting analysis. $**p < 0.01$ and $*p < 0.05$ when compared with controls

consequences of alcohol dependence (Macey et al. 1996; Liu and Weiss 2002, 2003; Moore et al. 2004; Budygin et al. 2007; Miki et al. 2008; Gilpin et al. 2009; Richardson et al. 2009; Zahr et al. 2009). However, little is known about the impact of CIE on neuron structure and function, and regenerative events in the prefrontal cortex (Weitlauf and Woodward 2008; Richardson et al. 2009; Holmes et al. 2012; Kroener et al. 2012), a brain region injured by alcohol abuse (Parsons and Nixon 1993; Sullivan et al. 2000; Bechara et al. 2001). Such investigations of chronic alcohol on mPFC neuron structure and development of glial progenitors could help clarify the relationship between neuron structure and gliogenesis in alcohol

dependence. The present results highlight how CIE alters the structure of pyramidal neurons in the mPFC via disrupting glial plasticity by reducing myelinating oligodendrocytes and myelin-associated proteins in the mPFC. Specifically, we demonstrate that CIE increases dendritic arborization and spine density within the basal and apical dendrites of pyramidal neurons with corresponding increases in the levels of the actin nucleator complex Arp2/3. CIE also increased the levels of NR2B subunits without significant changes in the phosphorylation state of NR2B at Tyr-1472 or levels of PSD-95. This suggests an aberrant relocation of NMDARs to extrasynaptic sites in the mPFC neurons that may contribute to synaptic activity and excitotoxic cell death in the mPFC. We also demonstrate that newly born progenitors in the mPFC differentiate into neurogenic bHLH transcription factor Olig2-expressing myelinating oligodendrocytes, and that CIE reduces the process of myelinating oligodendrogenesis by altering cell cycle kinetics of progenitors and inducing aberrant hyperphosphorylation of Olig2. The reduction in myelinating oligodendrogenesis is also associated with reduction of myelin basic protein in the mPFC in CIE animals. These effects of chronic alcohol exposure produced by the CIE paradigm on pyramidal neurons and myelin indicate one possible neurobiological alteration contributing to the pathology of alcohol dependence.

NMDA receptors in the mPFC are subject to dynamic regulation during ethanol exposure and during withdrawal from ethanol (Hu and Ticku 1997; Tsai and Coyle 1998; Chandler 2003; Prendergast and Mulholland 2012). For example, acute ethanol exposure inhibits NMDA receptor function (Tu et al. 2007; Weitlauf and Woodward 2008; Woodward and Pava 2009), and chronic ethanol exposure (via CIE) increases NMDA function and/or expression of NMDA receptors (Hu and Ticku 1995; Holmes et al. 2012; Kroener et al. 2012). CIE-induced NMDA receptor potentiation is hypothesized to be associated with the excitotoxic processes associated with CNS hyperexcitability during ethanol withdrawal episodes (Crews et al. 1996; Chandler et al. 1998). The mechanism(s) underlying CIE-induced adaptive changes in NMDARs are not clear, and could be associated with increases in NMDA receptor density, particularly functional changes in NMDARs (Hu and Ticku 1995; Chandler et al. 1998). Notably, functional changes in NMDARs are significantly linked with phosphorylation and dephosphorylation of NR2B subunits (Ali and Salter 2001; Nakazawa et al. 2001, 2006). For example, activity-dependent phosphorylation of Tyr-1472 by the Fyn family of tyrosine kinases is essential for proper localization of NR2B-containing receptors at synapses (Yaka et al. 2002; Lavezzari et al. 2003; Prybylowski et al. 2005; Nakazawa et al. 2006) and plays a mechanistic role in the behavioral and physiological tolerance produced by

ethanol (Miyakawa et al. 1997). Furthermore, phosphorylation of NR2B at Tyr-1472 and interactions of NR2B with PSD-95 regulate internalization of NMDARs via clathrin-mediated endocytosis, such that phosphorylation suppresses NMDAR endocytosis and dephosphorylation enhances NMDAR endocytosis (Lavezzari et al. 2003; Prybylowski et al. 2005). In this context, the acute effects of ethanol on reduced NMDA receptor activity in the hippocampus are associated with reduced phosphorylation of NR2B subunits at Tyr-1472 without significant changes in total NR2B levels (Alvestad et al. 2003), suggesting mislocalization of NR2B subunits and NMDARs by ethanol. Chronic ethanol exposure (via CIE) in mice increases NMDA receptor activity (Holmes et al. 2012; Kroener et al. 2012) and increases the expression of total NR2B (Kroener et al. 2012). The present findings in rats are consistent with the previous studies in mice and demonstrate that chronic CIE enhances expression of NR2B subunits in the mPFC, and significantly extend the findings to demonstrate that the increase in total NR2B receptor density is not associated with enhanced phosphorylation of NR2B at Tyr-1472 or enhanced levels of PSD-95. Altered NR2B levels, together with a lack of regulation from Fyn phosphorylation and PSD-95, suggests that during CIE, NR2B-containing NMDARs may relocate to extrasynaptic sites, contributing to the dysregulation of NMDAR activity associated with withdrawal and protracted abstinence (Clapp et al. 2010).

Dendritic arborization and spine density are forms of structural plasticity governed by intrinsic genetic programs and extrinsic signals, and are subject to dynamic regulation during CNS excitotoxicity (Smart and Halpain 2000; Cline 2001). For example, CIE in mice produces dendritic hypertrophy of mPFC neurons, suggesting significant dendritic remodeling in the mPFC (Holmes et al. 2012). While it has been demonstrated that alterations in neuron structure are not a prerequisite for neuron function (Lang et al. 2004), the abnormal structure of mPFC neurons in CIE animals correlated with deficits in mPFC neuronal function (Holmes et al. 2012; Kroener et al. 2012). The present findings in rats are consistent with previous studies in mice and demonstrate that chronic CIE in rats increases dendritic arborization of pyramidal neurons within the basal and apical dendrites, and significantly extend the findings to demonstrate that the increase in arborization is associated with an enhanced density of spines within the basal and apical dendrites of pyramidal neurons. Spine plasticity (generation and elimination) is regulated by NMDARs, but the precise consequences of NMDAR activation on spine pruning is variable and is under intense investigation (Smart and Halpain 2000; Cline 2001). In this context, aberrant NMDAR synaptic activity increases the number of spines (Kirov and Harris 1999) and such a

neuroadaptation could contribute to CIE-induced enhanced spine density within the apical and basal dendrites in mPFC pyramidal neurons. We next wanted to determine whether the enhanced spine density was associated with increased levels of specialized cytoskeleton molecules that are dedicated to maintaining structure, stability and activity of newly formed spines. For example, actin filament dynamics via actin-related proteins (Arp2 and Arp3) are known to be a key player in the formation of filaments on dendrites that elongate into protrusions and eventually form spine heads (Cooper and Schafer 2000). Notably, the interaction of Arp2/3 with other key players such as nWASP and PSD-95 is critical to functional mature spine formation (Wegner et al. 2008). Our findings of enhanced Arp2/3 levels without associated increases in nWASP and PSD-95 in CIE animals suggests immature spine formation following CIE. These biochemical findings are supported by detailed morphological characteristics of spines in CIE animals, which indicate a CIE enhancement of nonmushroom-type spines (Harris et al. 1992). Taken together, enhanced expression of NR2B subunits and aberrant arborization within basal and apical dendrites associated with enhanced formation of nonmushroom-type spines in the pyramidal neurons in the mPFC demonstrates a dysfunctional reorganization of prefrontal neuronal networks by CIE.

We have previously shown that CIE reduces the number of proliferating and surviving progenitors in the mPFC (Richardson et al. 2009). The present findings significantly extend our previous studies to demonstrate that CIE reduces the number of progenitors actively dividing in the S-phase of the cell cycle. CIE also reduces the length of the S-phase of the cell cycle, indicating a mechanism contributing to CIE-induced reduction in proliferation of glial progenitors in the mPFC. For example, it has been hypothesized that during development, regulation of cell cycle kinetics (such as length of time a cell spends in the cell cycle) controls the expansion versus differentiation of cortical neural progenitors (Bally-Cuif and Hammerschmidt 2003; Ohnuma and Harris 2003; Dehay and Kennedy 2007); such that reducing the length of the cell cycle assists with maintenance of the undifferentiated state (Lange et al. 2009; Salomoni and Calegari 2010). Furthermore, alterations in the length of G_1 phase of the cell cycle have been causally linked to the switch from proliferation to neurogenesis of cortical progenitors during development (Lange et al. 2009). In vitro models have demonstrated that increases in the length of S-phase of the cell cycle of human neuroblastoma cells corresponded to enhanced expression of neuronal differentiation markers (Guarnieri et al. 2009), suggesting that length of S-phase also regulates the fate of proliferating cells. These studies in developmental models and in vitro models have led to the hypothesis that shortening of the length of S-phase of

hippocampal neural progenitors by binge ethanol treatment in adolescent rats may result in reduced differentiation of hippocampal neural progenitors (McClain et al. 2011). Based on these studies, it appears that CIE-mediated reduction in the length of S-phase of mPFC progenitors may promote an expansion of the glial progenitor pool and maintain glial progenitors in an undifferentiated state.

In the postnatal brain, Olig2 (a bHLH transcription factor and a proneural factor with significant roles in gliogenesis) is expressed in premyelinating oligodendrocyte progenitors and in mature and terminally differentiating myelinating oligodendrocytes, where it appears to have ongoing biological functions (Rivers et al. 2008). During development, the function of Olig2 is dynamically modulated by regulated phosphorylation of a conserved triple serine motif (S10, 13 and 14) within the amino-terminal domain (Sun et al. 2011). For example, phosphorylation status of the triple serine motif of Olig2 undergoes a dramatic decrease as proliferating progenitors in the embryo mature into terminally differentiated, myelinating oligodendrocytes (Sun et al. 2011). These findings suggest a positive correlation between hyperphosphorylation of Olig2 and diminished differentiation of Olig2 progenitors into terminally differentiated myelinating oligodendrocytes and myelin. In this context, CIE produced hyperphosphorylation of Olig2 and concomitantly reduced the number of differentiating premyelinating oligodendrocytes (BrdU+/Olig2+) and the levels of myelin in the mPFC. These results, combined with altered cell cycle kinetics of proliferating progenitors provide a relationship between CIE-induced reduction in myelin and altered structure of pyramidal neurons.

Collectively, these data propose that CIE produces an abnormal structure of pyramidal neurons in the mPFC, with accompanying abnormalities in gliogenesis, myelinating oligodendrogenesis and myelin. The finding that the structure of pyramidal neurons is vulnerable to CIE via alterations in myelin plasticity implies that a chronic history of alcohol abuse may increase the risk of maladaptive cognitive and emotional behaviors dependent on the PFC via myelin loss.

References

Ali DW, Salter MW (2001) NMDA receptor regulation by Src kinase signalling in excitatory synaptic transmission and plasticity. Curr Opin Neurobiol 11:336–342

Allen NJ, Barres BA (2009) Neuroscience: Glia—more than just brain glue. Nature 457:675–677

Alvestad RM, Grosshans DR, Coultrap SJ, Nakazawa T, Yamamoto T, Browning MD (2003) Tyrosine dephosphorylation and ethanol inhibition of N-Methyl-D-aspartate receptor function. J Biol Chem 278:11020–11025

Bally-Cuif L, Hammerschmidt M (2003) Induction and patterning of neuronal development, and its connection to cell cycle control. Curr Opin Neurobiol 13:16–25

Bava S, Jacobus J, Thayer RE, Tapert SF (2013) Longitudinal changes in white matter integrity among adolescent substance users. Alcohol Clin Exp Res 37(Suppl 1):E181–E189

Bechara A, Dolan S, Denburg N, Hindes A, Anderson SW, Nathan PE (2001) Decision-making deficits, linked to a dysfunctional ventromedial prefrontal cortex, revealed in alcohol and stimulant abusers. Neuropsychologia 39:376–389

Belachew S, Chittajallu R, Aguirre AA, Yuan X, Kirby M, Anderson S, Gallo V (2003) Postnatal NG2 proteoglycan-expressing progenitor cells are intrinsically multipotent and generate functional neurons. J Cell Biol 161:169–186

Breunig JJ, Silbereis J, Vaccarino FM, Sestan N, Rakic P (2007) Notch regulates cell fate and dendrite morphology of newborn neurons in the postnatal dentate gyrus. Proc Natl Acad Sci USA 104:20558–20563

Budygin EA, Oleson EB, Mathews TA, Lack AK, Diaz MR, McCool BA, Jones SR (2007) Effects of chronic alcohol exposure on dopamine uptake in rat nucleus accumbens and caudate putamen. Psychopharmacology 193:495–501

Burns KA, Kuan CY (2005) Low doses of bromo- and iododeoxyuridine produce near-saturation labeling of adult proliferative populations in the dentate gyrus. Eur J Neurosci 21:803–807

Butt AM, Kiff J, Hubbard P, Berry M (2002) Synantocytes: new functions for novel NG2 expressing glia. J Neurocytol 31:551–565

Cameron HA, McKay RD (2001) Adult neurogenesis produces a large pool of new granule cells in the dentate gyrus. J Comp Neurol 435:406–417

Chandler LJ (2003) Ethanol and brain plasticity: receptors and molecular networks of the postsynaptic density as targets of ethanol. Pharmacol Ther 99:311–326

Chandler LJ, Harris RA, Crews FT (1998) Ethanol tolerance and synaptic plasticity. Trends Pharmacol Sci 19:491–495

Clapp P, Gibson ES, Dell'acqua ML, Hoffman PL (2010) Phosphorylation regulates removal of synaptic N-methyl-D-aspartate receptors after withdrawal from chronic ethanol exposure. J Pharmacol Exp Ther 332:720–729

Cline HT (2001) Dendritic arbor development and synaptogenesis. Curr Opin Neurobiol 11:118–126

Cooper JA, Schafer DA (2000) Control of actin assembly and disassembly at filament ends. Curr Opin Cell Biol 12:97–103

Crews FT, Morrow AL, Criswell H, Breese G (1996) Effects of ethanol on ion channels. Int Rev Neurobiol 39:283–367

Dawson MR, Polito A, Levine JM, Reynolds R (2003) NG2-expressing glial progenitor cells: an abundant and widespread population of cycling cells in the adult rat CNS. Mol Cell Neurosci 24:476–488

De Bellis MD, Narasimhan A, Thatcher DL, Keshavan MS, Soloff P, Clark DB (2005) Prefrontal cortex, thalamus, and cerebellar volumes in adolescents and young adults with adolescent-onset alcohol use disorders and comorbid mental disorders. Alcohol Clin Exp Res 29:1590–1600

Dehay C, Kennedy H (2007) Cell-cycle control and cortical development. Nat Rev Neurosci 8:438–450

Edwards S, Vendruscolo LF, Schlosburg JE, Misra KK, Wee S, Park PE, Schulteis G, Koob GF (2012) Development of mechanical hypersensitivity in rats during heroin and ethanol dependence: alleviation by CRF(1) receptor antagonism. Neuropharmacology 62:1142–1151

Edwards S, Baynes BB, Carmichael CY, Zamora-Martinez ER, Barrus M, Koob GF, Gilpin NW (2013) Traumatic stress reactivity promotes excessive alcohol drinking and alters the balance of prefrontal cortex-amygdala activity. Transl Psychiatry 3:e296

Fields RD (2005) Myelination: an overlooked mechanism of synaptic plasticity? Neuroscientist 11:528–531

Fields RD (2010) Neuroscience. Change in the brain's white matter. Science 330:768–769

George MS, Anton RF, Bloomer C, Teneback C, Drobes DJ, Lorberbaum JP, Nahas Z, Vincent DJ (2001) Activation of prefrontal cortex and anterior thalamus in alcoholic subjects on exposure to alcohol-specific cues. Arch Gen Psychiatry 58:345–352

Gilpin NW, Richardson HN, Cole M, Koob GF (2008) Vapor inhalation of alcohol in rats. Curr Protoc Neurosci Chapter 9: Unit 9 29

Gilpin NW, Smith AD, Cole M, Weiss F, Koob GF, Richardson HN (2009) Operant behavior and alcohol levels in blood and brain of alcohol-dependent rats. Alcohol Clin Exp Res 33:2113–2123

Gould E, Woolley CS, Frankfurt M, McEwen BS (1990) Gonadal steroids regulate dendritic spine density in hippocampal pyramidal cells in adulthood. J Neurosci 10:1286–1291

Grant KA, Valverius P, Hudspith M, Tabakoff B (1990) Ethanol withdrawal seizures and the NMDA receptor complex. Eur J Pharmacol 176:289–296

Guarnieri S, Pilla R, Morabito C, Sacchetti S, Mancinelli R, Fano G, Mariggio MA (2009) Extracellular guanosine and GTP promote expression of differentiation markers and induce S-phase cell-cycle arrest in human SH-SY5Y neuroblastoma cells. Int J Dev Neurosci 27:135–147

Harris KM, Jensen FE, Tsao B (1992) Three-dimensional structure of dendritic spines and synapses in rat hippocampus (CA1) at postnatal day 15 and adult ages: implications for the maturation of synaptic physiology and long-term potentiation. J Neurosci 12:2685–2705

Hayes NL, Nowakowski RS (2000) Exploiting the dynamics of S-phase tracers in developing brain: interkinetic nuclear migration for cells entering versus leaving the S-phase. Dev Neurosci 22:44–55

Hayes NL, Nowakowski RS (2002) Dynamics of cell proliferation in the adult dentate gyrus of two inbred strains of mice. Brain Res Dev Brain Res 134:77–85

Heilig M, Egli M (2006) Pharmacological treatment of alcohol dependence: target symptoms and target mechanisms. Pharmacol Ther 111:855–876

Holmes A, Fitzgerald PJ, MacPherson KP, DeBrouse L, Colacicco G, Flynn SM, Masneuf S, Pleil KE, Li C, Marcinkiewcz CA, Kash TL, Gunduz-Cinar O, Camp M (2012) Chronic alcohol remodels prefrontal neurons and disrupts NMDAR-mediated fear extinction encoding. Nat Neurosci 15:1359–1361

Hu XJ, Ticku MK (1995) Chronic ethanol treatment upregulates the NMDA receptor function and binding in mammalian cortical neurons. Brain Res Mol Brain Res 30:347–356

Hu XJ, Ticku MK (1997) Functional characterization of a kindling-like model of ethanol withdrawal in cortical cultured neurons after chronic intermittent ethanol exposure. Brain Res 767:228–234

Hu XJ, Follesa P, Ticku MK (1996) Chronic ethanol treatment produces a selective upregulation of the NMDA receptor subunit gene expression in mammalian cultured cortical neurons. Brain Res Mol Brain Res 36:211–218

Jacobus J, McQueeny T, Bava S, Schweinsburg BC, Frank LR, Yang TT, Tapert SF (2009) White matter integrity in adolescents with histories of marijuana use and binge drinking. Neurotoxicol Teratol 31:349–355

Jurgens HA, Amancherla K, Johnson RW (2012) Influenza infection induces neuroinflammation, alters hippocampal neuron morphology, and impairs cognition in adult mice. J Neurosci 32:3958–3968

Kang SH, Fukaya M, Yang JK, Rothstein JD, Bergles DE (2010) NG2+ CNS glial progenitors remain committed to the oligodendrocyte lineage in postnatal life and following neurodegeneration. Neuron 68:668–681

Kirov SA, Harris KM (1999) Dendrites are more spiny on mature hippocampal neurons when synapses are inactivated. Nat Neurosci 2:878–883

Kroener S, Mulholland PJ, New NN, Gass JT, Becker HC, Chandler LJ (2012) Chronic alcohol exposure alters behavioral and synaptic plasticity of the rodent prefrontal cortex. PLoS One 7:e37541

Lang C, Barco A, Zablow L, Kandel ER, Siegelbaum SA, Zakharenko SS (2004) Transient expansion of synaptically connected dendritic spines upon induction of hippocampal long-term potentiation. Proc Natl Acad Sci USA 101:16665–16670

Lange C, Huttner WB, Calegari F (2009) Cdk4/cyclinD1 overexpression in neural stem cells shortens G1, delays neurogenesis, and promotes the generation and expansion of basal progenitors. Cell Stem Cell 5:320–331

Lavezzari G, McCallum J, Lee R, Roche KW (2003) Differential binding of the AP-2 adaptor complex and PSD-95 to the C-terminus of the NMDA receptor subunit NR2B regulates surface expression. Neuropharmacology 45:729–737

Lewohl JM, Wixey J, Harper CG, Dodd PR (2005) Expression of MBP, PLP, MAG, CNP, and GFAP in the human alcoholic brain. Alcohol Clin Exp Res 29:1698–1705

Ligon KL, Kesari S, Kitada M, Sun T, Arnett HA, Alberta JA, Anderson DJ, Stiles CD, Rowitch DH (2006) Development of NG2 neural progenitor cells requires Olig gene function. Proc Natl Acad Sci USA 103:7853–7858

Liu X, Weiss F (2002) Additive effect of stress and drug cues on reinstatement of ethanol seeking: exacerbation by history of dependence and role of concurrent activation of corticotropin-releasing factor and opioid mechanisms. J Neurosci 22:7856–7861

Liu X, Weiss F (2003) Stimulus conditioned to foot-shock stress reinstates alcohol-seeking behavior in an animal model of relapse. Psychopharmacology 168:184–191

Macey DJ, Schulteis G, Heinrichs SC, Koob GF (1996) Time-dependent quantifiable withdrawal from ethanol in the rat: effect of method of dependence induction. Alcohol 13:163–170

MacKay RK, Colson NJ, Dodd PR, Lewohl JM (2011) Differential expression of 14-3-3 isoforms in human alcoholic brain. Alcohol Clin Exp Res 35:1041–1049

Mandyam CD, Koob GF (2012) The addicted brain craves new neurons: putative role for adult-born progenitors in promoting recovery. Trends Neurosci 35:250–260

Mandyam CD, Norris RD, Eisch AJ (2004) Chronic morphine induces premature mitosis of proliferating cells in the adult mouse subgranular zone. J Neurosci Res 76:783–794

Mandyam CD, Wee S, Eisch AJ, Richardson HN, Koob GF (2007) Methamphetamine self-administration and voluntary exercise have opposing effects on medial prefrontal cortex gliogenesis. J Neurosci 27:11442–11450

Markham JA, McKian KP, Stroup TS, Juraska JM (2005) Sexually dimorphic aging of dendritic morphology in CA1 of hippocampus. Hippocampus 15:97–103

Maslov AY, Barone TA, Plunkett RJ, Pruitt SC (2004) Neural stem cell detection, characterization, and age-related changes in the subventricular zone of mice. J Neurosci 24:1726–1733

McClain JA, Hayes DM, Morris SA, Nixon K (2011) Adolescent binge alcohol exposure alters hippocampal progenitor cell proliferation in rats: effects on cell cycle kinetics. J Comp Neurol 519:2697–2710

McQueeny T, Schweinsburg BC, Schweinsburg AD, Jacobus J, Bava S, Frank LR, Tapert SF (2009) Altered white matter integrity in adolescent binge drinkers. Alcohol Clin Exp Res 33:1278–1285

Medina KL, McQueeny T, Nagel BJ, Hanson KL, Schweinsburg AD, Tapert SF (2008) Prefrontal cortex volumes in adolescents with alcohol use disorders: unique gender effects. Alcohol Clin Exp Res 32:386–394

Miki T, Kuma H, Yokoyama T, Sumitani K, Matsumoto Y, Kusaka T, Warita K, Wang ZY, Hosomi N, Imagawa T, SBedi K, Itoh S, Nakamura Y, Takeuchi Y (2008) Early postnatal ethanol exposure induces fluctuation in the expression of BDNF mRNA in the developing rat hippocampus. Acta Neurobiol Exp (Wars) 68:484–493

Miyakawa T, Yagi T, Kitazawa H, Yasuda M, Kawai N, Tsuboi K, Niki H (1997) Fyn-kinase as a determinant of ethanol sensitivity: relation to NMDA-receptor function. Science 278:698–701

Moore DB, Madorsky I, Paiva M, Barrow Heaton M (2004) Ethanol exposure alters neurotrophin receptor expression in the rat central nervous system: effects of neonatal exposure. J Neurobiol 60:114–126

Nakazawa T, Komai S, Tezuka T, Hisatsune C, Umemori H, Semba K, Mishina M, Manabe T, Yamamoto T (2001) Characterization of Fyn-mediated tyrosine phosphorylation sites on GluR epsilon 2 (NR2B) subunit of the N-methyl-D-aspartate receptor. J Biol Chem 276:693–699

Nakazawa T, Komai S, Watabe AM, Kiyama Y, Fukaya M, Arima-Yoshida F, Horai R, Sudo K, Ebine K, Delawary M, Goto J, Umemori H, Tezuka T, Iwakura Y, Watanabe M, Yamamoto T, Manabe T (2006) NR2B tyrosine phosphorylation modulates fear learning as well as amygdaloid synaptic plasticity. EMBO J 25:2867–2877

Noori HR, Fornal CA (2011) The appropriateness of unbiased optical fractionators to assess cell proliferation in the adult hippocampus. Front Neurosci 5:140

Nowakowski RS, Lewin SB, Miller MW (1989) Bromodeoxyuridine immunohistochemical determination of the lengths of the cell cycle and the DNA-synthetic phase for an anatomically defined population. J Neurocytol 18:311–318

O'Dell LE, Roberts AJ, Smith RT, Koob GF (2004) Enhanced alcohol self-administration after intermittent versus continuous alcohol vapor exposure. Alcohol Clin Exp Res 28:1676–1682

Ohnuma S, Harris WA (2003) Neurogenesis and the cell cycle. Neuron 40:199–208

Olariu A, Cleaver KM, Cameron HA (2007) Decreased neurogenesis in aged rats results from loss of granule cell precursors without lengthening of the cell cycle. J Comp Neurol 501:659–667

Parsons OA, Nixon SJ (1993) Neurobehavioral sequelae of alcoholism. Neurol Clin 11:205–218

Paxinos G, Watson C (1997) The rat brain in stereotaxic coordinates, 3rd edn. Academic Press, San Diego

Peters A, Kaiserman-Abramof IR (1970) The small pyramidal neuron of the rat cerebral cortex. The perikaryon, dendrites and spines. Am J Anat 127:321–355

Pfefferbaum A, Sullivan EV (2005) Disruption of brain white matter microstructure by excessive intracellular and extracellular fluid in alcoholism: evidence from diffusion tensor imaging. Neuropsychopharmacology 30:423–432

Prendergast MA, Mulholland PJ (2012) Glucocorticoid and polyamine interactions in the plasticity of glutamatergic synapses that contribute to ethanol-associated dependence and neuronal injury. Addict Biol 17:209–223

Prybylowski K, Chang K, Sans N, Kan L, Vicini S, Wenthold RJ (2005) The synaptic localization of NR2B-containing NMDA receptors is controlled by interactions with PDZ proteins and AP-2. Neuron 47:845–857

Richardson HN, Lee SY, O'Dell LE, Koob GF, Rivier CL (2008) Alcohol self-administration acutely stimulates the hypothalamic-pituitary-adrenal axis, but alcohol dependence leads to a dampened neuroendocrine state. Eur J Neurosci 28:1641–1653

Richardson HN, Chan SH, Crawford EF, Lee YK, Funk CK, Koob GF, Mandyam CD (2009) Permanent impairment of birth and survival of cortical and hippocampal proliferating cells following excessive drinking during alcohol dependence. Neurobiol Dis 36:1–10

Ridge JP, Ho AM, Innes DJ, Dodd PR (2008) The expression of NMDA receptor subunit mRNA in human chronic alcoholics. Ann N Y Acad Sci 1139:10–19

Rimondini R, Sommer W, Heilig M (2003) A temporal threshold for induction of persistent alcohol preference: behavioral evidence in a rat model of intermittent intoxication. J Stud Alcohol 64:445–449

Rivers LE, Young KM, Rizzi M, Jamen F, Psachoulia K, Wade A, Kessaris N, Richardson WD (2008) PDGFRA/NG2 glia generate myelinating oligodendrocytes and piriform projection neurons in adult mice. Nat Neurosci 11:1392–1401

Roberts AJ, Heyser CJ, Cole M, Griffin P, Koob GF (2000) Excessive ethanol drinking following a history of dependence: animal model of allostasis. Neuropsychopharmacology 22:581–594

Salomoni P, Calegari F (2010) Cell cycle control of mammalian neural stem cells: putting a speed limit on G1. Trends Cell Biol 20:233–243

Schulteis G, Markou A, Cole M, Koob GF (1995) Decreased brain reward produced by ethanol withdrawal. Proc Natl Acad Sci USA 92:5880–5884

Seo D, Lacadie CM, Tuit K, Hong KI, Constable RT, Sinha R (2013) Disrupted ventromedial prefrontal function, alcohol craving, and subsequent relapse risk. JAMA Psychiatry 70:727–739

Skuja S, Groma V, Smane L (2012) Alcoholism and cellular vulnerability in different brain regions. Ultrastruct Pathol 36:40–47

Smart FM, Halpain S (2000) Regulation of dendritic spine stability. Hippocampus 10:542–554

Sommer WH, Rimondini R, Hansson AC, Hipskind PA, Gehlert DR, Barr CS, Heilig MA (2008) Upregulation of voluntary alcohol intake, behavioral sensitivity to stress, and amygdala crhr1 expression following a history of dependence. Biol Psychiatry 63:139–145

Squeglia LM, Pulido C, Wetherill RR, Jacobus J, Brown GG, Tapert SF (2012) Brain response to working memory over 3 years of adolescence: influence of initiating heavy drinking. J Stud Alcohol Drugs 73:749–760

Sullivan EV, Rosenbloom MJ, Pfefferbaum A (2000) Pattern of motor and cognitive deficits in detoxified alcoholic men. Alcohol Clin Exp Res 24:611–621

Sun Y, Meijer DH, Alberta JA, Mehta S, Kane MF, Tien AC, Fu H, Petryniak MA, Potter GB, Liu Z, Powers JF, Runquist IS,

Rowitch DH, Stiles CD (2011) Phosphorylation state of Olig2 regulates proliferation of neural progenitors. Neuron 69:906–917

Tapert SF, Brown GG, Baratta MV, Brown SA (2004a) fMRI BOLD response to alcohol stimuli in alcohol dependent young women. Addict Behav 29:33–50

Tapert SF, Pulido C, Paulus MP, Schuckit MA, Burke C (2004b) Level of response to alcohol and brain response during visual working memory. J Stud Alcohol 65:692–700

Tsai G, Coyle JT (1998) The role of glutamatergic neurotransmission in the pathophysiology of alcoholism. Annu Rev Med 49:173–184

Tu Y, Kroener S, Abernathy K, Lapish C, Seamans J, Chandler LJ, Woodward JJ (2007) Ethanol inhibits persistent activity in prefrontal cortical neurons. J Neurosci 27:4765–4775

Valdez GR, Roberts AJ, Chan K, Davis H, Brennan M, Zorrilla EP, Koob GF (2002) Increased ethanol self-administration and anxiety-like behavior during acute ethanol withdrawal and protracted abstinence: regulation by corticotropin-releasing factor. Alcohol Clin Exp Res 26:1494–1501

Vega CJ, Peterson DA (2005) Stem cell proliferative history in tissue revealed by temporal halogenated thymidine analog discrimination. Nat Methods 2:167–169

Vendruscolo LF, Barbier E, Schlosburg JE, Misra KK, Whitfield TW Jr, Logrip ML, Rivier C, Repunte-Canonigo V, Zorrilla EP, Sanna PP, Heilig M, Koob GF (2012) Corticosteroid-dependent plasticity mediates compulsive alcohol drinking in rats. J Neurosci 32:7563–7571

Watanabe M, Toyama Y, Nishiyama A (2002) Differentiation of proliferated NG2-positive glial progenitor cells in a remyelinating lesion. J Neurosci Res 69:826–836

Wegner AM, Nebhan CA, Hu L, Majumdar D, Meier KM, Weaver AM, Webb DJ (2008) N-wasp and the arp2/3 complex are critical regulators of actin in the development of dendritic spines and synapses. J Biol Chem 283:15912–15920

Weitlauf C, Woodward JJ (2008) Ethanol selectively attenuates NMDAR-mediated synaptic transmission in the prefrontal cortex. Alcohol Clin Exp Res 32:690–698

Woodward JJ, Pava MJ (2009) Effects of ethanol on persistent activity and up-States in excitatory and inhibitory neurons in prefrontal cortex. Alcohol Clin Exp Res 33:2134–2140

Yaka R, Thornton C, Vagts AJ, Phamluong K, Bonci A, Ron D (2002) NMDA receptor function is regulated by the inhibitory scaffolding protein, RACK1. Proc Natl Acad Sci USA 99:5710–5715

Yuan CJ, Quiocho JM, Kim A, Wee S, Mandyam CD (2011) Extended access methamphetamine decreases immature neurons in the hippocampus which results from loss and altered development of neural progenitors without altered dynamics of the S-phase of the cell cycle. Pharmacol Biochem Behav 100:98–108

Zahr NM, Mayer D, Vinco S, Orduna J, Luong R, Sullivan EV, Pfefferbaum A (2009) In vivo evidence for alcohol-induced neurochemical changes in rat brain without protracted withdrawal, pronounced thiamine deficiency, or severe liver damage. Neuropsychopharmacology 34:1427–1442

Zhao Y, Weiss F, Zorrilla EP (2007) Remission and resurgence of anxiety-like behavior across protracted withdrawal stages in ethanol-dependent rats. Alcohol Clin Exp Res 31:1505–1515